Thermal, Dynamic-Mechanical, and Dielectric Properties of Surfactant Intercalated Graphite Oxide Filled Maleated Polypropylene Nanocomposites

Yeh Wang, Huai-B. Tsai

Department of Chemical Engineering, Tunghai University, Taichung, Taiwan 407, Republic of China

Received 3 November 2010; accepted 24 May 2011
DOI 10.1002/app.34976
Published online 2 September 2011 in Wiley Online Library (wileyonlinelibrary.com).

ABSTRACT: Graphite oxide (GO) and amine surfactant intercalated graphite oxide (GOS) filled maleated polypropylene (PPgMA) nanocomposites were prepared directly by solution blending. In this study, the effects of the surfactant intercalation on the crystalline structure, thermo-mechanical, and dielectric properties of PPgMA/GO and GOS composites are reported. Wide-angle X-ray diffraction exhibited a lower intensity diffraction peak of the monoclinic (α) phase of PPgMA for PPgMA/GOS composites compared with the unfilled sample. Differential scanning calorimetry exhibited a single characteristic melting peak of monoclinic (α) crystalline phase. The incorporation of GOS hardly showed any change in T_m. However, the significant decrease in the melting enthalpy of PPgMA/GOS composite, which was lower than that of GO filled PPgMA, demonstrated the high degree of dispersion of the GOS flakes in the PPgMA matrix. Dynamical mechanical analysis indicated that incorporation of GO or GOS into PPgMA increased both the storage modulus and the glass transition temperature, due to the hydrogen bonding between GO and the maleic anhydride group of PPgMA. Dielectric analyzer showed significant increase in both dielectric permittivity and dielectric loss at high temperature regimes in the GOS nanocomposites. The finely dispersed GOS in the PPgMA matrix manifested the interfacial polarization, which gave rise to much greater ε′ and ε″ than that of PPgMA/GO hybrid. © 2011 Wiley Periodicals, Inc. J Appl Polym Sci 123: 3154–3163, 2012

Key words: polypropylene; nanocomposite; graphite oxide; intercalation

INTRODUCTION

Commercial exploitation of isotactic polypropylene has been expanded rapidly due to its attractive characters of low cost, low weight, heat distortion temperature above 100°C, and extraordinary versatility in terms of properties, applications, and recycling. The addition of nanoscopic fillers of high anisotropy, instead of acting as conventional reinforcing agents, enhances a wide range of performance by the polypropylene nanocomposites, such as mechanical, thermal, and conductive properties, at a relatively small loading.[1] The most common nanoreinforcements used are layered silicate nanoclays and carbon nanotubes; however, graphite platelets are also among the leading nanoscale fillers in research development and commercial projects.[2] As demonstrated recently by various research groups,[3–6] exfoliated graphite nanoplatelets, which combine the lower price and layered structure of clays with the superior thermal and electrical properties of carbon nanotubes, can be an effective alternative to both clays and nanotubes and provide excellent, competitive, and functional properties.

Graphite is a layered mineral composed of weakly bonded graphene sheets which are held together by van der Waals forces with a large aspect ratio. Single crystal graphite is one of the stiffest materials in nature with an elastic modulus of over 1 TPa, which is many times greater than nanoclay. Unlike clay, graphite is thermally and electrically conductive. It also has a lower density than clay. Graphite has been known as a host material for many chemicals, including metal halides, metal oxides, and mineral acids.[7–9] Traditionally, oxidation of the natural graphite yields expandable graphite, which is also called acid-intercalated graphite flake. It can be expanded up to hundreds of times over its initial volume at high temperature, resulting in separation of the graphene sheets at the nanoscopic level along the c-axis of graphene layers.[5,10–12] Nonetheless, the CO_2 over-pressure due to rapid heating at high temperature may distort aromatic ring structures of graphite oxide (GO) and lead to deterioration of mechanical and conductive properties.[13] This study aims to investigate the chemical exfoliation of GO, which can be performed in a suspension at mild temperatures and hence upscalability is straightforward, offers a route to large scale graphene production.[14]

Correspondence to: Y. Wang (yehwang@thu.edu.tw).
Contract grant sponsor: NSC of Taiwan; contract grant number: NSC-97-2221-E-029-001.

GO is characterized to be a lamellar solid with unoxidized aromatic regions and aliphatic regions containing phenolic, carboxyl, and epoxide groups as a result of oxidation.[15] Thus, the GO platelets are strongly hydrophilic and dispersible in neutral water.[16] Although delamination of GO in aqueous media is well characterized,[17] the dispersion of GO in organic solvents has not been well explored. Only with organically intercalated GO, is it possible to form monolayer colloidal dispersion in organic solvents, which would help in the preparation of GO composites with polymer species that are insoluble in water. Alkyltrimethyl ammonium ion intercalated GO have been dissolved in organic solvents by a few authors.[18–20] However, systematic investigations on the delamination behavior of amine intercalated GO and the preparation of its composites has not been reported so far.

Recent research has shown that exfoliated graphite nanoplatelets, which combines the layered structure of nanoclays with the electrical and thermal properties comparable with that of carbon nanotubes, are very cost-effective and can provide a variety of physical and chemical property enhancements. It is expected that superior thermal transport properties of nanographite dispersion have potential for composite structural applications and thermal management in miniaturized electronic devices.[21] The production of electrically conductive polyolefin[21,22] can be used, for example, for electromagnetic shielding and antistatic coating. On the other hand, maleated polypropylene (PPgMA) has long been used as a compatibilizer in commercial blends and composites.[23–25] In view of the success of the layered nanocomposites of PPgMA and clay[26] or graphite,[27,28] we attempted in this study to prepare the conducting nanocomposites of surfactant intercalated graphite oxide (GOS) with PPgMA via solution blending. The goal of this research is to explore the effect of GOS on the thermal, mechanical, and conductive properties, of the nanocomposites. The results presented here are thermal and mechanical properties from dynamical mechanical analysis (DMA), the thermal conductivity from differential scanning calorimetry (DSC), and the dielectrical properties and the electric conductivity from dielectric analyzer (DEA).

EXPERIMENTAL

Materials

PPgMA, M_w = 330,000 (PB3150, Chemtru), 99% synthetic graphite (SG, Aldrich), 90% octadecylamine (ODA, Acros), certified 99.8% *p*-xylene (Tedia), sulfuric acid synthesis grade (Scharlau, Spain), potassium permanganate regent grade (Showa, Japan), and hydrogen peroxide regent grade (Showa, Japan) were used as received. All aqueous solutions were prepared in deionized water obtained by purification with a Sartorius Arium 611 system.

Chemical oxidation of graphite

The method due to Hummers and Offeman[29] was adopted to prepare GO from SG powder through chemical oxidation[30] in the presence of concentrated sulfuric acid and potassium permanganate. The solid GO was separated by centrifugation, washed repeatedly with deionized water and acetone until sulfate could not be detected with $BaCl_2$ and dried overnight in an airoven at 65°C. The dried GO powder is mainly composed of layered but compactly fastened nanoplatelets of graphite.

Intercalation of GO with amine surfactant

Based on previous investigations,[31–33] the neutral surfactant, ODA of 99% (Acros), was used in this study. In each case, a sample of 100 mg of GO was dispersed in 200 mL of *p*-xylene in a glass beaker, followed by the addition of 400 mg of ODA amine. On amine addition, the GO solid swelled instantly. Each mixture was allowed to stir for 3 h at room temperature using an ultrasonic processor VCX750 (Sonics & Materials), frequency 20 kHz, 750 W, equipped with a medium probe made of high grade titanium alloy. The stable dispersion of surfactant intercalated GO (GOS) was observed over 24 h.

Solution-blended PPgMA/graphite nanocomposites

Appropriate amount of PPgMA were completely dissolved in *p*-xylene in a 250 mL glass beaker on heating to 105°C, and subsequently the heated GOS suspension was added dropwise. After stirring for 5 h, a significant portion of *p*-xylene was removed under vacuum, and the well dispersed blend was cooled to 70°C. The separation of the resulting derivatives was achieved with a suction filter to remove the excess ODA and *p*-xylene. Finally, the precipitate was washed well with acetone, and then dried *in vacuo* at 100°C for 48 h. The resulting loose powder was hot pressed to produce the testing specimens. The composition of each composite was confirmed by thermal gravimetric analysis at 5 wt % of graphite filler. The choice of 5 wt % loading is based on our experimental results, in which the calculated direct current conductivity was 10^{-5} S m^{-1} (30°C) at 5% loading of GOS, which was well above that (10^{-11} S m^{-1}) of the percolation point at ca. 1% loading, though the results are not reported in this article.

Characterization

Wide-angle X-ray diffraction (WAXD) patterns of different samples were recorded on a Schimadzu

XRD-6000 (40 kV/40 mA) diffractometer using Cu Kα radiation to characterize the nano-graphite dispersion and the crystalline structure of PPgMA. Infrared spectra were recorded on a Schimadzu FT-IR spectrometer (Prestige-21) to identify the chemical groups of graphite due to oxidation and intercalation. The samples were measured in the form of KBr pellets. SEM images of the morphology of GO and GOS powders were observed by field-emission scanning electron microscope (FESEM) JSM-6400 (JEOL, Japan) with accelerating voltage of 12 kV and working distance of 15 mm. The dispersion of graphite particles within the PPgMA matrix was also studied by SEM. The freeze-fractured sample surfaces were metallized with platinum using an ion coater IB-3 (Giko, Japan). Transmission electron microscopy (TEM) JEM-1200EX (JEOL, Japan) was used for direct observation of the intercalated lamellar structure of graphite oxide in the nanocomposites. Ultrathin samples were obtained by microtoming the sample plates.

Thermal properties of the composites were characterized using a Perkin-Elmer DSC Pyris 1 (Perkin Elmer, Boston, MA). Thermal conductivity measurements were preformed on the same DSC following the previous procedures.[21,34] DMA, Perkin–Elmer 7e, was used to assess the mechanical performance of the composites. For the dielectric measurements of the pristine PB3150 and the nanocomposites covering the temperature range from 30°C to 130°C and the frequency range from 1 to 10^4 Hz were performed with a TA high-performance dielectric spectrometer DEA 2970.

RESULTS AND DISCUSSION

Structural evolution of GO and GOS (ODA intercalated GO)

Preliminarily, a characterization of the filler was performed. The structure of the filler was investigated under a scanning electron microscope, shown in Figure 1(a–c) for the graphite flakes of SG, GO, and GOS, respectively, after the sonicated dispersion dried on a glass for 24 h. It can be seen from Figure 1 that most graphite flakes were fragmented under prolonged oxidation and ultrasonication, and produced graphite sheets with diameters ranging from about 1 to 10 μm. The starting material is the neat SG in the form of thick plate as shown in Figure 1(a). The arithmetic means of the particle dimensions were obtained by averaging at least 20 particles from the micrographs taken at different regions of the same specimen. Note that the GO flake [Fig. 1(b)], with the thickness less than 0.2 μm, is apparently thinner than that of SG due to oxidative intercalation. Furthermore, the intercalating effect of ODA can be clearly seen in Figure 1(c), where the stack of graphite sheet was exfoliated into thin plates, whose average thickness was around 80 nm, were generally thinner than that of GO.

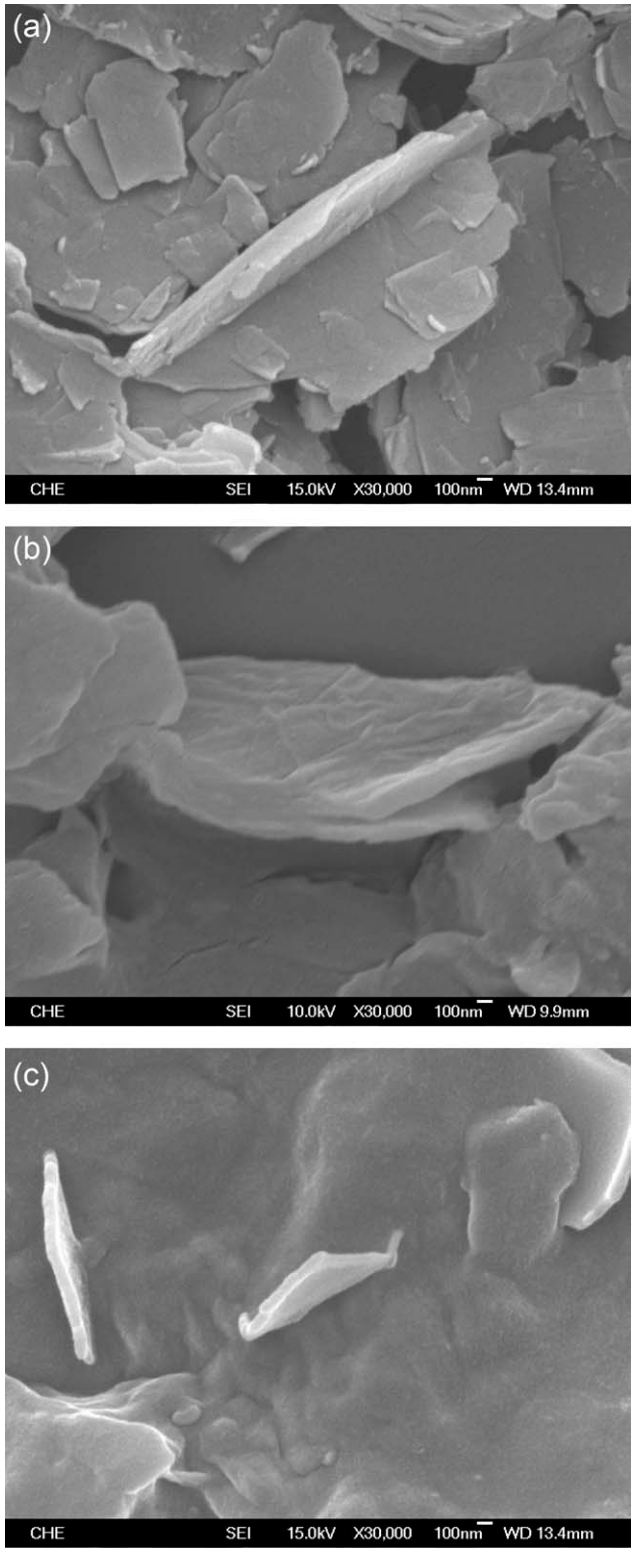

Figure 1 SEM micrographs of (a) SG; (b) GO; and (c) GOS (× 30,000).

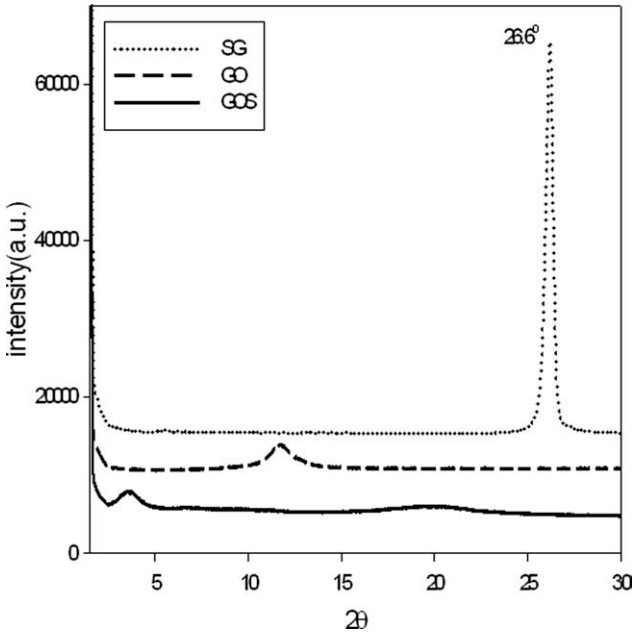

Figure 2 WAXD patterns of (a) SG; (b) GO; and (c) GOS.

The powder X-ray diffraction patterns of GOS, the as prepared alkylamine intercalated GO, are compared with that of the neat SG and GO in Figure 2. As expected, SG has a prominent, characteristic peak at $2\theta = 26.6^\circ$, corresponding to an inter-graphene sheet spacing of 0.34 nm. However, the diffraction peak of GO shifted to the left of SG due to the effect of oxidative intercalation. The interlayer spacing was increased to 0.75 nm in GO. Furthermore, compared with the parent GO, in the alkylamine intercalated samples, GOS, the diffraction peak shifted further to the left. There is an apparent increase of the d_{001} value up to 23.5 nm for ODA intercalated GO. The increased value confirms the incorporation of the ODA molecules in the interlayer space of GO. The amine molecules could be inserted in the interlayer zone of GO either by hydrogen bonding interactions between amine molecules and oxygen containing functional groups of GO or by exchange of protons of the acidic groups of GO with alkylamines or due to amine nucleophilic attack on the epoxy groups of GO.[32]

The intercalation of GO was also confirmed by infrared spectroscopy. FTIR spectra of GO and GOS (ODA intercalated GO) are presented in Figure 3. The spectrum of GO is in good agreement with previous works.[32,33] The broad band at 3400 cm^{-1} is attributed to stretching of the O-H bond of CO-H or water. The band at 1723 cm^{-1} is associated with stretching of the C=O bond of carbonyl or carboxyl groups. The band present at 1600 cm^{-1} is attributed to deformations of the O-H bending vibration in water. Stretching vibrations of the C-O bond is observed as the intense band present at 1060 cm^{-1}. The FTIR spectra of GOS differ from that of GO in the signals observed at 1060, 1470, 1570, 2924, and 2850 cm^{-1}. The intensity of the first peak is reduced significantly. The next two peaks are assigned to the bending vibration of —CH2—, and vibration of the N-H groups of the intercalants, respectively. The strongest signals, observed at higher frequencies, are attributed to asymmetric (2924 cm^{-1}) and symmetric (2850 cm^{-1}) stretching of the methylene group of the alkylamine. Note that rather weak absorption band for N-H stretching may overlap with the broad absorption of O-H around 3400 cm^{-1}. Furthermore, the reduction in interlayer water content in GOS is also confirmed from the fact that the intensities of the peaks at 3400 cm^{-1} and 1600 cm^{-1} clearly decrease compared with that of GO.

Morphology of polymer/graphite nanocomposites

Figure 4(a,c,e) are the images of the cryogenically fractured surfaces of composites of SG, GO, and GOS at 5 wt % loading, respectively, with low magnification of 1000×; and Figure 4(b,d,f) at high magnification of 5000×. It can be clearly seen that the fractured surface of Figure 4(e) is more homogeneous than that in Figure 4(a,c). As shown by the arrows in Figure 4, the images of the graphite flakes appear a little darker than the surrounding PPgMA, and most of the GOS flakes are embedded in the PPgMA matrix [see Fig. 4(c)]. Indeed, agglomeration of the SG and GO particles was more apparent than the GOS ones. It indicates the uniform dispersion of the intercalated graphite nanoplatelets in the composites, which has good adhesion between the constituents. In addition, as can be seen from Figure 4(b), SG can either bend/buckle or agglomerate in response to the shear condition they experienced in the sonication bath during solution blending. The high degree of agglomeration is attributable to the larger size of SG, which is more

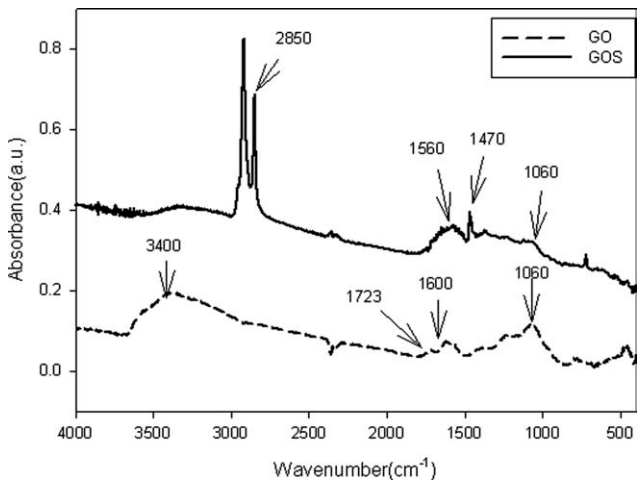

Figure 3 IR spectra of GO and GOS.

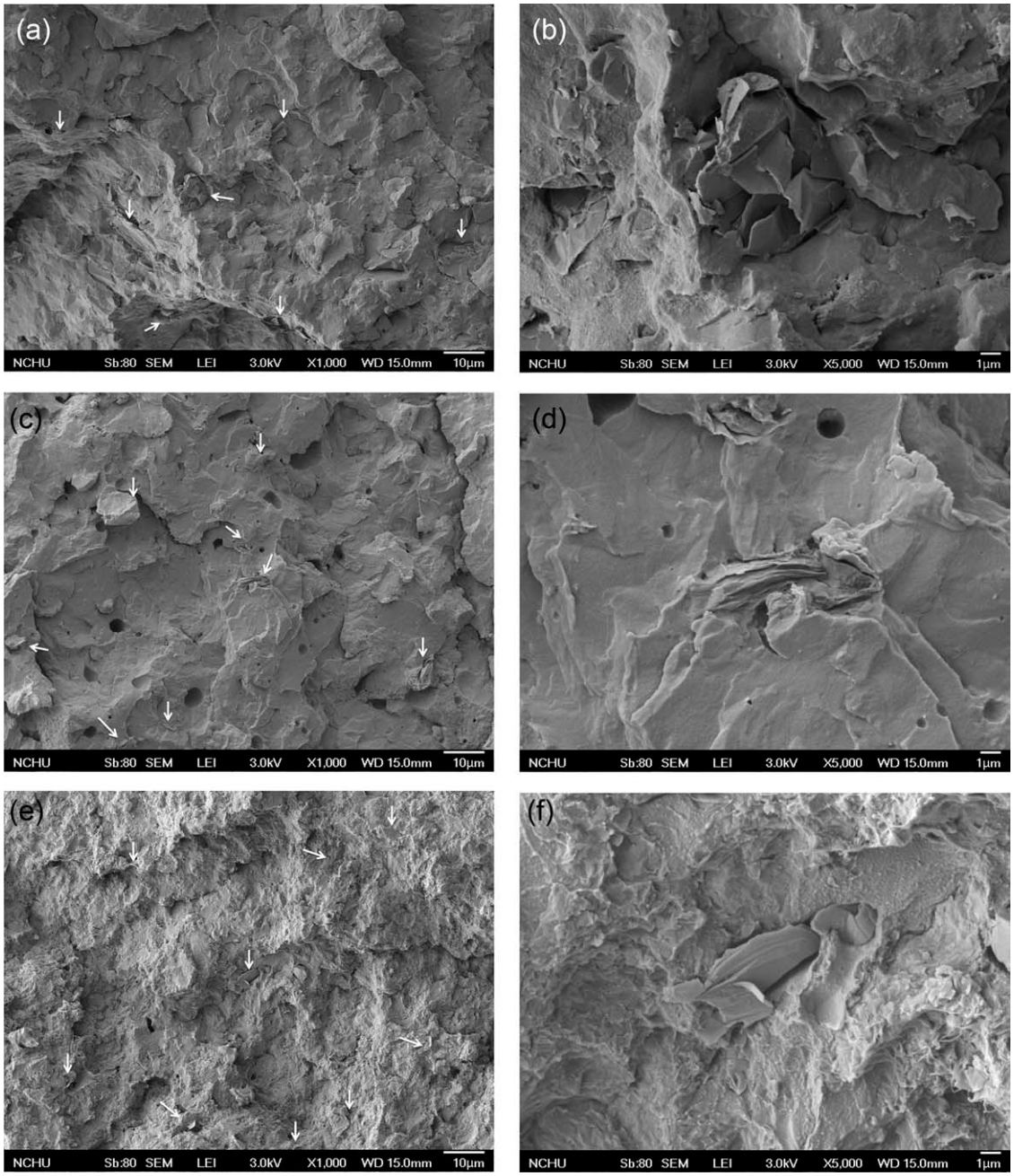

Figure 4 SEM micrographs of the cryogenically fractured surfaces of the nanocomposites at 5 wt % loading. (a) PB3150/SG at 1000×; (b) PB3150/SG at 5000×; (c) PB3150/GO at 1000×; (d) PB3150/GO at 5000×; (e) PB3150/GOS at 1000×; and (f) PB3150/GOS at 5000×.

flexible compared with the stiffer smaller GO and GOS, and hence more susceptible to out of plane bending during processing resulting in loss of its platelet morphology within the polymer matrix. The edge-on view of the nanoplatelets of both GO and GOS can be clearly seen from the high magnification images of 5000× in Figure 4(d,f), which shows the thickness of the flakes is about the same order as that shown in Figure 1.

Figures 5(a,b) show the repeatable and representative TEM micrographs of the PPgMA composites with 5 wt % GO and GOS nanoplatelets, respectively. As shown in Figure 5, the original graphite stacks of GO and GOS were partially exfoliated into a thinner multilayered structure or even nanolayers. As a result, no discernable diffraction peak was shown in the corresponding XRD patterns (see Fig. 6). The dark or gray sections and the bright domains are referred to as the intercalated graphite sheets and the polymer matrix, respectively. Furthermore, the dark stripes representative of the aggregated graphite layers of GO in Figure 5(a) are clearly

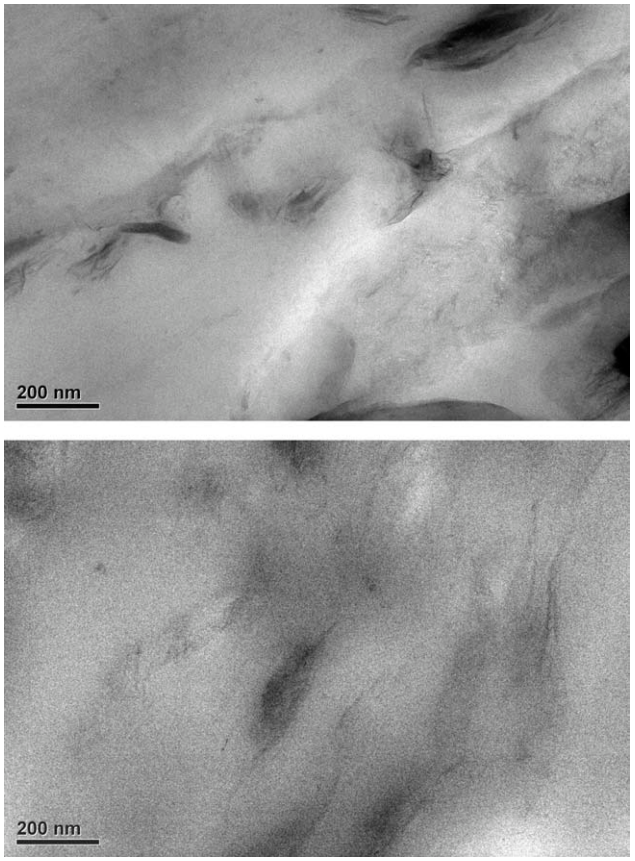

Figure 5 TEM micrographs of nanocomposites at 5 wt % loading. (a) PB3150/GO and (b) PB3150/GOS (×120,000).

thicker than that of GOS in Figure 5(b). As for the GOS nanocomposites, it can be seen that there exist a group or several groups of parallel graphite sheets (shown as thin gray lines) with a thickness of 10 nm approximately and a gallery of intercalated stacks (shown as expanded gray stripes) about 90 nm on average, finely dispersed in the PPgMA matrix, which is in good agreement with the previous literatures about nylon 6/EG nanocomposites prepared via intercalation polymerization method.[35] This demonstrates the effect of ODA intercalation, leading to the significant improvement of the interfacial adhesion between GOS and PPgMA matrix.

We also used XRD to further characterize graphite dispersion in the composites samples. In nanocomposites containing organoclay, increasing exfoliation is associated with a reduction of the peak intensity in XRD characteristic of the repeated layer spacing. We apply this same principle in graphite-based samples. As seen in Figure 6, the X-ray diffractograms of neat PB3150 and the PPgMA-graphite hybrids made by solution blending. Neat PB3150 has several XRD peaks between $2\theta = 15.0°$ and 28.3°, consistent with the PP crystal unit cell.[36,37] All the PPgMA-graphite systems exhibit peaks associated with neat PP, although the peak intensities are decreased in the hybrid. However, while the PPgMA/SG hybrid exhibits a diffraction peak at 26.6°, the peak associated with the inter-graphene sheet spacing is almost totally suppressed in the PPgMA/GO and GOS samples. This strongly suggests that significant exfoliation/dispersion of the GO and GOS flakes was achieved under ultrasonication. The X-ray diffraction results supplement the morphological observations from electronic microscopy.

DSC and thermal conductivity measurements

Figure 7 shows the DSC cooling [Fig. 7(a)] and heating [Fig. 7(b)] curves of PPgMA and the PPgMA composites. In Table I, we summarized the values of the temperature and enthalpy of crystallization and melting. The values of ΔHc and ΔHm were normalized by the weight content of PPgMA in the composite. The *Tc* values of all the PPgMA composites increased about 13°C compared with that of neat PPgMA. This was due to the nucleating effect of graphite on the PPgMA crystallization. However, compared with the DSC cooling curves of the PPgMA composites, the crystallization of PPgMA in PPgMA/GOS was faster than those in PPgMA/GO and the PPgMA/SG, as the DSC peak temperature for the former was a little higher than those of the latter, which indicated that GOS had a better nucleating effect on the crystallization of PPgMA than GO. Accordingly, the degree of crystallinity (ΔHc and ΔHm) of PPgMA in the composites is in the descending order as follows: PPgMA/SG > GO > GOS. The lowest ΔHc and ΔHm and the highest *Tc*

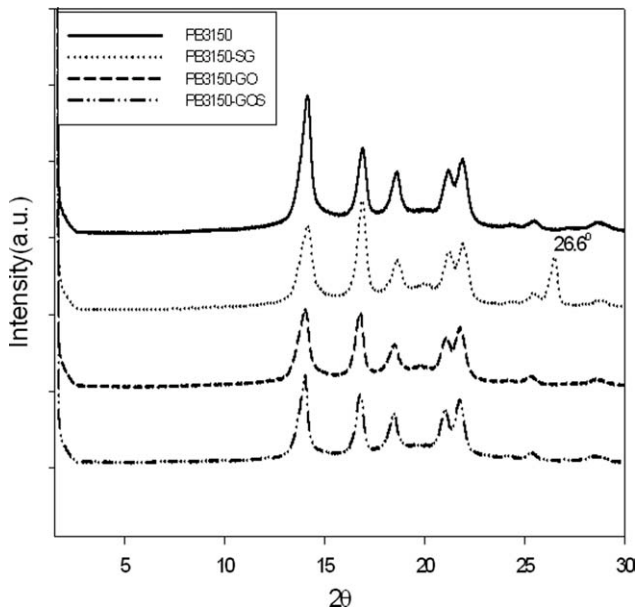

Figure 6 WAXD patters of neat PB3150 and composites at 5 wt % loading.

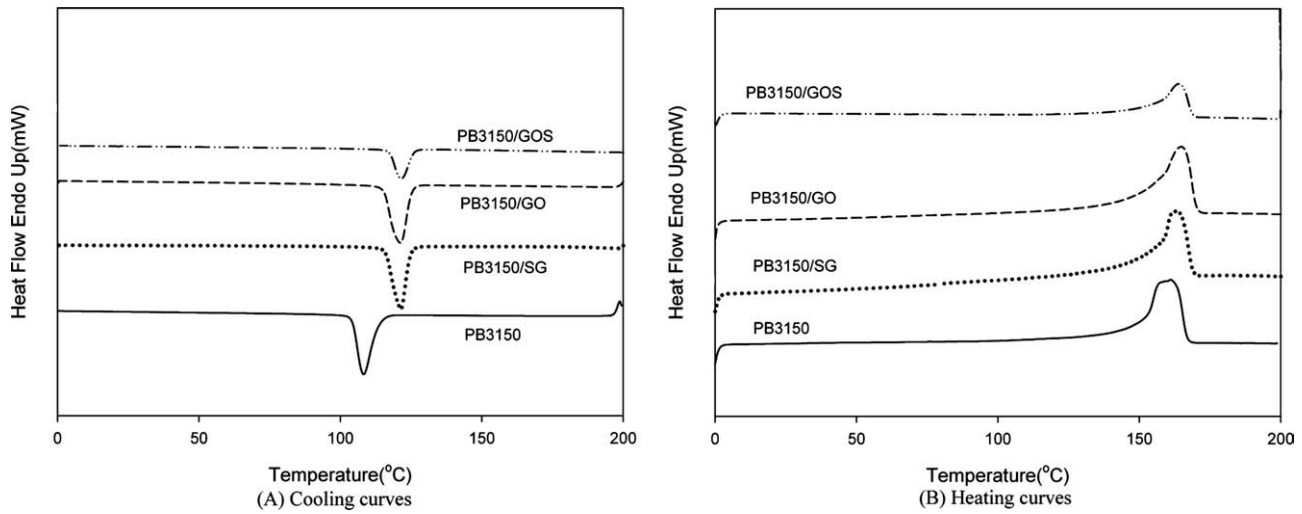

Figure 7 DSC thermograms of PPgMA and nanocomposites (a) cooling curves and (b) heating curves at 5 wt % loading.

observed for the PPgMA/GOS composite point to the apparent effect of nucleation, which could be probably attributed to the enhanced interfacial interaction between PPgMA and GOS resulting from the great increase in the specific surface area of GOS after dispersion/exfoliation in the sonication bath.

The thermal conductivity reported is the average value of three samples cut from different specimens. The melting curves of pure gallium (m.p. at 29.8°C) with different samples are shown in Figure 8. Note that the gallium-DSC method used here is limited to the through-plane conductivity.[21] As expected, the melting of gallium with the PPgMA/GOS nanocomposite started at a lower temperature (ca. 30°C) than other hybrid samples. The GOS filled sample yielded the steepest melting curve, corresponding to the highest thermal conductivity (ca. 0.29 W/m/°C), compared with that of neat resin ca. 0.16 W/m/°C, among the hybrid systems due to a higher aspect ratio of the width to the thickness of the graphite nanoplatelets and hence a smaller contribution from thermal contact resistance. As only the through-plane conductivities were measured here, they were much lower than the in-plane thermal conductivity of graphite is 210–230 W/m/°C. In addition, the morphology of PPgMA/graphite composites should also be taken into account. Morphological examination of the composites indicated that these large platelets were not very well dispersed and showed evidence of agglomeration as indicated in Figures 4 and 5. Additionally, the graphite platelets were not planar but were buckled or rolled-up into cylinders as shown in Figure 4(b,c), respectively, which reduced the aspect ratio and changed the assumed platelet geometry. Finally, it should be noted that the method used, i.e., using the slope of a heat flux vs. temperature plot obtained by DSC of the gallium-composite sample, becomes less sensitive at higher thermal conductivities. In any case, the method is sufficient for screening experiments of low filler contents with thermal conductivity lower than 1.2–1.5 W/m/°C.

TABLE I
Thermal Properties of PPgMA and PPgMA Nanocomposites

Sample	*Tm* (°C)	Δ*Hm* (J/g)	*Tc* (°C)	Δ*Hc* (J/g)
PB3150	161.1	115.8	108.3	−99.77
PB3150/SG	163.3	111.0	121.3	−105.8
PB3150/GO	164.8	99.2	121.1	−93.9
PB3150/GOS	164.1	81.2	121.7	−88.7

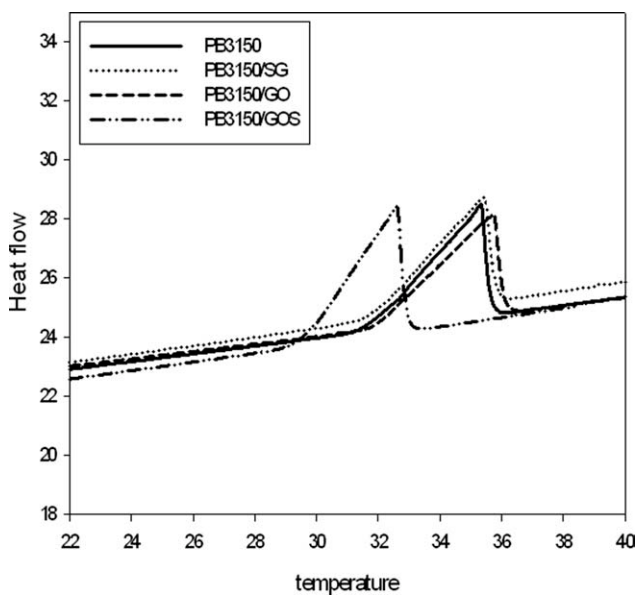

Figure 8 DSC melting curves of gallium with variations in thermal conductivities of neat PB3150 and composites at 5 wt % loading.

Dynamic mechanical thermal analysis

The dynamic mechanical behavior of unfilled PPgMA and PPgMA/graphite nanocomposites are presented in Figure 9(a,b). The storage (or elastic) moduli (E') are presented in Figure 9(a). The E' values of all the samples at nominated temperatures are listed in Table II. From the E' curves, it is apparent that in the presence of graphite fillers, the E' of the composites was greater than that of unfilled PPgMA, throughout the temperature range. The maximum of the glassy E' of filled PPgMA at −50°C was observed at 5 wt % for PPgMA filled with GOS. It increased from 390 MPa (unfilled PPgMA) to 430 MPa (PPgMA/GOS), which is higher than that of PPgMA filled with either SG (361 MPa) or GO (401 MPa).

Whilst the E' of filled PPgMA increased with subsequent additions the graphite and its oxide, it was found that the reinforcing effect is more prominent in PPgMA/GOS than PPgMA/GO. The lower E' of PPgMA/GO is believed to be attributed to the greater concentration of graphite stacks (as a result of mild intercalation due to oxidation) than that of PPgMA/GOS. This overabundance of GO stacks results in some filler particles being unable to bond to MA substituents. The glass transition (Tg), which is the viscoelastic transition of a material, is often drawn from the maxima of E'' curve as shown in Figure 9(b). In this case, the E'' curves were used to obtain the Tg. The Tg of the unfilled PPgMA is approximately 4.0°C. It can be clearly seen that the Tg's of the nanocomposites are higher than that of unfilled PPgMA. Similar to the trend of E', the Tg of PPgMA/GOS is the highest at 6.0°C, followed by PPgMA/GO at 5.3°C, and PPgMA/SG is even lower at 4.2°C. The increase in Tg is ascribed to a decrease in mobility of the polymer chains, due to the strong interactions, hydrogen bonding between the polar groups of PPgMA and GO or GOS. This observation is also consistent with the behavior of other filled polymeric systems.[38]

TABLE II
Dynamic Storage Moduli and Glass Transition Temperature of Unfilled PPgMA and PPgMA/Graphite Nanocomposites at Nominal Temperatures

Sample	E' (MPa)				Tg (°C)
	−50°C	−30°C	−10°C	30°C	
PB3150	373	360	332	209	3.44
PB3150/SG	409	389	353	211	3.51
PB3150/GO	404	388	354	216	3.97
PB3150/GOS	467	437	389	233	4.63

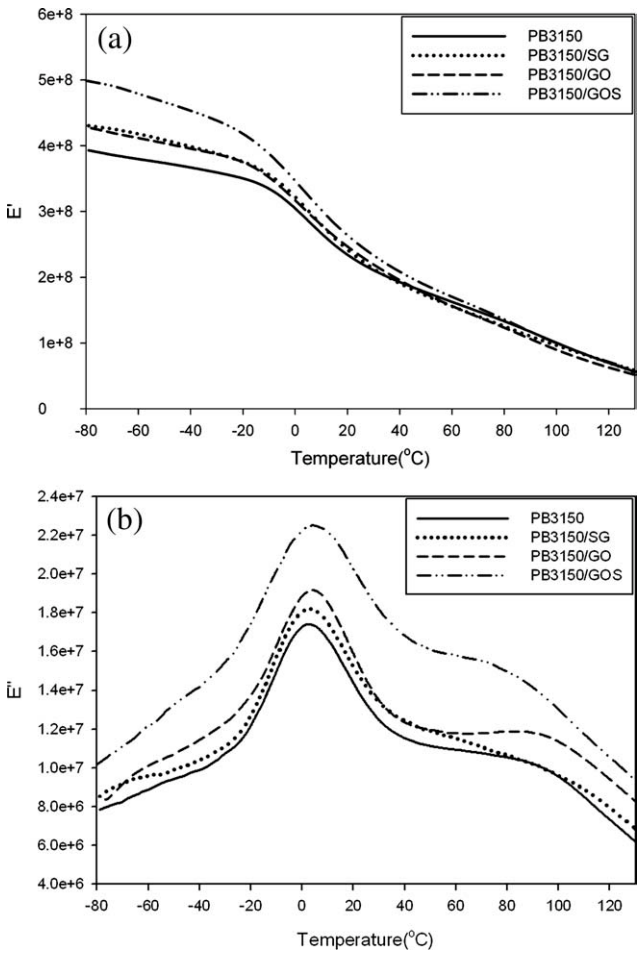

Figure 9 (a) Storage modulus curves of neat PB3150 and composites at 5 wt % loading as a function of temperature. (b) Loss modulus curves of neat PB3150 and composites at 5 wt % loading as a function of a temperature.

Dielectric spectroscopy analysis

The dielectric measurements of the neat PB3150 and its nanocomposites of 5 wt % SG, GO, and GOS, extending over a temperature range from −50°C to 140°C at 100 Hz, are shown in Figure 10(a,b). As can be seen form Figure 10(a), the dielectric constant, ε', of neat resin remains as a constant at 2.2, showing no dielectrically active relaxation process regardless of its low grafting degree of the maleic anhydride. The hybrids of SG and GO filled PPgMA display the similar response except that the magnitudes of ε' become slightly larger than unfilled PPgMA. However, the ε' of PPgMA/GOS is not only the largest among the composites but also increases significantly with increasing temperature.

As the ε'' of unfilled PPgMA nearly vanishes due to the nonpolar nature of PP backbone, and the SG filled PPgMA also shows negligible ε'' because of the high purity SG hardly possessing any charge carriers, we only present the dielectric loss, ε'', of the two samples, i.e., GO and GOS filled PPgMA in Figure 10(b). As expected, the ε'' of PPgMA/GOS is much larger than that of PPgMA/GO, and the

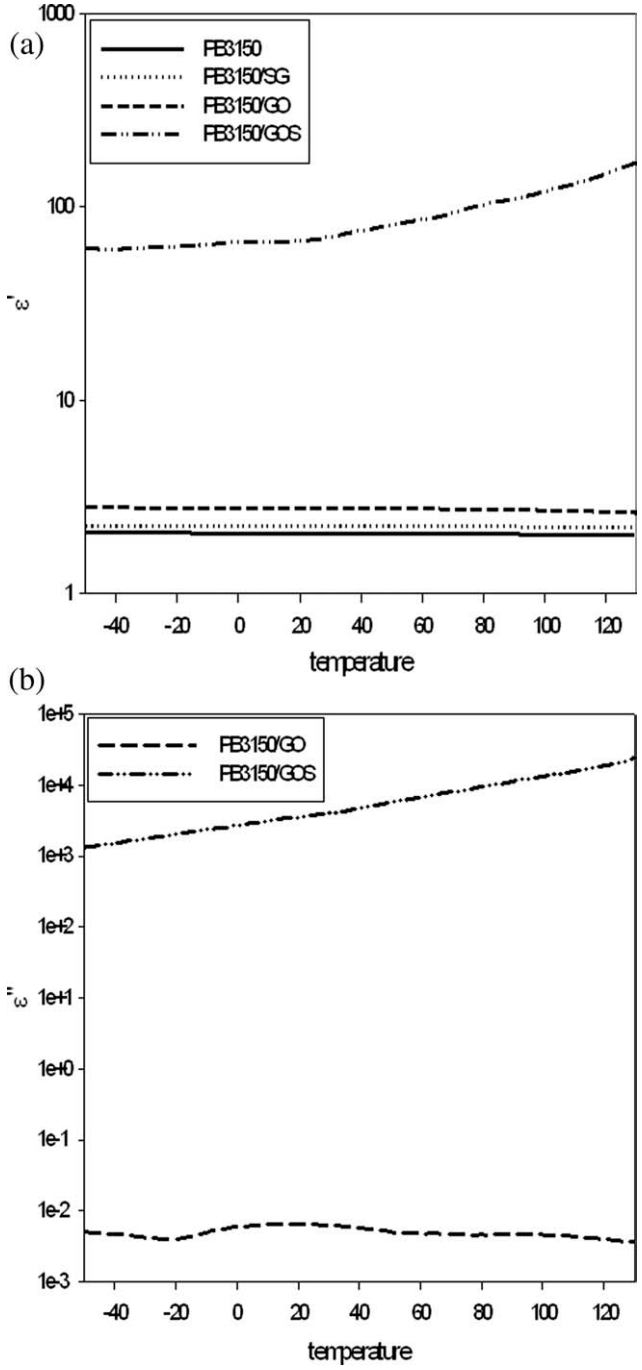

Figure 10 (a) Temperature sweep curves of dielectric permittivity for neat PB3150 and composites at 5 wt % loading at 100 Hz. (b) Temperature sweep curves of dielectric loss for PB3150/GO and PB3150/GOS at 5 wt % loading at 100 Hz.

difference becomes more significant at high temperature regions. Furthermore, while the ε'' curve of the GO filled composite remains flat, the ε'' of the GOS composite increases significantly at high temperatures. The modification of GO through the addition of the ODA increased the interlayer spacing of the intercalated graphite layered stacks and facilitated the exfoliation of the graphite nanolayers in the PPgMA/GOS composites. Note that the molecular interaction between the polymer chain segments and nanolayers is greatly enhanced in the PPgMA/GOS hybrids due to enormous increase in the interfacial area.[39] Hence, in this configuration, the heterogeneous graphite nanolayer inclusions often cause dielectric polarization as a result of the accumulation of charge carriers at the interface of two media with different permittivities or conductivities. Therefore, it can form an effective nanosized capacitor structure[40,41] and provide increased values of bulk permittivity and loss factor in such a nanostructured morphology.

CONCLUSION

The addition of amine surfactant was found to significantly affect the layered structure and increase the surface area of GOS (i.e., the intercalated GO). As evidenced by XRD, GO was well intercalated in the presence of ODA. The diffraction peaks of the inter-graphene sheet spacing shifted to the lower angles after intercalation. The electron microscopic studies clearly showed that the thickness of GOS flakes has been reduced compared to that of GO after ultrasonication. Additionally, the WAXD analysis of PPgMA/GO and GOS composites exhibited α crystalline peaks; however, the peak intensity were lower than that of unfilled PPgMA. The results were consistent with the DSC analysis, where the melting enthalpies of the composites were lower than the neat resin. The interlayer spacing of graphite layers found no alteration when it was incorporated into the PPgMA matrix. This indicates that the graphite layers were both ordered and multilayered within the PPgMA matrix, a conclusion which was confirmed by electron microscopy.

The thermal conductivities, k, were determined with the DSC method. The k value of PPgMA/GOS hybrid appeared to be the highest (nearly 80% increase relative to the pur PPgMA) among the composite systems under investigation. Note that degree of exfoliation, orientation, and interfacial interaction have an influence on the thermal transport in composites. The interfacial interactions between PPgMA and GOS were improved by the long alkyl chain of ODA intercalant. However, unlike the exponential increase in electrical conductivity, thermal conductivity enhancement by GOS is not as dramatic. This is partly due to smaller contrast in thermal conductivity between polymers and graphitic carbons.

The dynamic mechanical properties indicated that GO and GOS had a reinforcing effect on the elastic behavior of PPgMA. The composite materials with 5 wt % GOS loading exhibited the highest G' and Tg. This was thought to be due to the ease of PPgMA diffusing into the gallery of GOS. The confined polymer chains in the gallery were not free from chain

motion through the hydrogen bonding of polar groups in the individual constituents. The superior properties of PPgMA/GOS system reflect the compatibility between the GOS nanoplatelets and the PPgMA matrix.

Finally, a significant increase of the dielectric permittivity and dielectric loss was observed for the PPgMA/GOS system because the dispersive GOS, with larger surface-to-volume ratio than GO, contributed to the space charge polarization which caused the great increase in both ε' and ε'' at the high temperatures beyond *Tg*. The direct current electrical conductivity of the PPgMA/GOS hybrid, σ_{dc}, calculated from ε'', was also the largest among the PPgMA/graphite composites. The 5 wt % loading of GOS can be seen well beyond the percolation threshold. The improvement in σ_{dc} of PPgMA/GOS clearly demonstrated a high degree of dispersion of GOS and compatibility with the polymer matrix. These results can be further optimized by enhancing the adhesion at the GOS–PPgMA interface, and by improving the dispersion and orientation of the graphite nanoplatelets by selecting appropriate processing methods. Overall, exfoliated nanoplatelets have demonstrated an exciting new ability to simultaneously improve multiple physical, thermal, and mechanical properties of polymer composites making GOS a multifunctional nanoreinforcement.

REFERENCES

1. Gibson, A. G. In Polypropylene:Structure, Blends and Composites, Vol. 3, Karger-Kocsis, J., Ed.; Chapman & Hall: London, 1995; Chapter 2, pp 71–112.
2. Sherman, L. M. Chasing Nanocomposites. Plastics Technology. Available at: http://www.plasticstechnology.com/articles/200411fa2.html. Accessed November, 2004.
3. Wakabayashi, K.; Pierre, C.; Dikin, D. A.; Ruoff, R. S.; Ramanathan, T.; Brinson, L.C.; Torkelson, J. M. Macromolecules 2008, 41, 1905.
4. Kim, H.; Macosko, C. W. Macromolecules 2008, 41, 3317.
5. Kalaitzidou, K.; Fukushima, H.; Drzal, L. T.; Compos Sci Technol 2007, 67, 2045.
6. Wong, S.-C.; Sutherland, E. M.; Uhl, F. M. Materials and Manufacturing Processes 2006, 20, 159.
7. Chung, D. D. L. J Mater Sci 2002, 37, 1475.
8. Dresselhaus, M. S. Phys Today 1984, 37, 60.
9. Shioyama, H. Synth Met 2000, 114, 1.
10. Chen, G.-H.; Wu, D.J.; Weng, W. G.; Yan, W. L. J Appl Polym Sci 2001, 82, 2506.
11. Zheng, W.-G.; Wong, S.-C.; Sue, H.-J. Polymer 2002, 43, 6767.
12. Uhla, F. M.; Yao, Q.; Nakajima, H.; Manias, E.; Wilkie, C. A. Polym Degrad Stab 2005, 89, 70.
13. Lerf, A.; He, H.; Forster, M.; Klinowski, J. J Phys Chem B 1998, 102, 4477.
14. Park, S.; Ruoff, R. S. Nat Nanotechnol 2009, 4, 217.
15. He, H.; Klinowski, J.; Forster, M.; Lerf, A. Chem Phys Lett 1998, 287, 53.
16. Croft, R. C. Q Rev 1960, 14, 1.
17. Thiele, H. Kolloid-Z 1948, 111, 15.
18. Matsuo, Y.; Fukutsuka, T.; Sugie, Y. Carbon 2002, 40, 958.
19. Matsuo, Y.; Hatase, K.; Sugie, Y. Chem Lett 1999, 10, 1109.
20. Matsuo. Y.; Hatase, K.; Sugie, Y. Chem Commun 1999, 35, 43.
21. Kalaitzidou, K.; Fukushima, H.; Drzal, L. T. Carbon 2007, 45, 1446.
22. Steurer, P.; Wissert, R.; Thomann, R.; Muelhaupt, R. Macromol Rapid Commun 2009, 30, 316.
23. Gartner, C.; Suarez, M.; Lopez, B. L. Polym Eng Sci 2008, 48, 1910.
24. Kim, H.-S., Lee, B.-H., Choi, S.-W., Kim, S., Kim, H.-J. Compos A, 2007, 38, 1473.
25. Chemtura. Polybond Technical Report, 2004.
26. Wang, Y.; Huang, S.-W. Polym Plast Technol Eng 2007, 46, 1039.
27. Shen, J.-W.; Chen, X.-M.; Huang, W.-Y. J Appl Polym Sci 2003, 88, 1864.
28. Cerezo, F. T.; Preston, C. M. L.; Shanks, R. A. Macromol Mater Eng 2007, 292, 155.
29. Hummers, W. S.; Offeman, R. E. J Am Chem Soc 1958, 8, 1339.
30. Weiss, A. Angew Chem Int Ed Engl 1981, 20, 850.
31. Matsuo, Y.; Niwa, T.; Sugie, Y. Carbon 1999, 37, 897.
32. Bourlinos, A. B.; Gournis, D.; Petridis, D.; Szabo, T.; Szeri, A.; Dekany, I. Langmuir 2003, 19, 6050.
33. Nethravathi, C.; Rajamathi, M. Carbon 2006, 44, 2635.
34. Khanna, Y. P.; Taylor, J. P.; Chomyn, G. Polym Eng Sci 1988, 28, 1034.
35. Pan, Y.-X.; Yu, Z.-Z.; Qu, Y.-C.; Hu, G.-H. J Polym Sci Part B: Polym Phys 2000, 38, 1626.
36. Saujanya, C.; Radhakrishnan, S. Polymer 2001, 42, 6723.
37. Gopakumar, T. G.; Page, D. J. Y. S. Polym Eng Sci 2004, 44, 1162.
38. Zheng, W.; Wong, S. C. Compos Sci Technol 2003, 63, 225.
39. Roy, A. S.; Anilkumar, K. R. J Appl Polym Sci 2011, 121, 675.
40. Williams, E. P. M.; Seferis, J. C.; Wittman, C. L.; Parker, G. A.; Lee, J. H.; Nam, J.-D. J Polym Sci Part B: Polym Phys 2004, 42, 1.
41. Wang, Y.; Huang, S.-W.; Guo, J.-Y. e-Polymers 2008, 075, 1.